

Dynamic Phase Transitions in Cell Spreading

Hans-Günther Döbereiner, Benjamin Dubin-Thaler, Grégory Giannone, Harry S. Xenias, and Michael P. Sheetz
*Department of Biological Sciences, Columbia University, New York, NY 10027 **

We monitored isotropic spreading of mouse embryonic fibroblasts on fibronectin-coated substrates. Cell adhesion area versus time was measured via total internal reflection fluorescence microscopy. Spreading proceeds in well-defined phases. We found a power-law area growth with distinct exponents a_i in three sequential phases, which we denote basal ($a_1 = 0.4 \pm 0.2$), continuous ($a_2 = 1.6 \pm 0.9$) and contractile ($a_3 = 0.3 \pm 0.2$) spreading. High resolution differential interference contrast microscopy was used to characterize local membrane dynamics at the spreading front. Fourier power spectra of membrane velocity reveal the sudden development of periodic membrane retractions at the transition from continuous to contractile spreading. We propose that the classification of cell spreading into phases with distinct functional characteristics and protein activity patterns serves as a paradigm for a general program of a phase classification of cellular phenotype. Biological variability is drastically reduced when only the corresponding phases are used for comparison across species/different cell lines.

PACS numbers: 05.45.-a, 87.17.-d

Cells need to be mobile in order to perform many critical biological functions. The reorganization of extracellular matrix in wound healing, the positioning of nerve cells, or the engulfment of bacteria in the immune reaction of white blood cells are particular examples [1]. Accomplishing this variety of functions requires a diverse set of mechanisms and proteins. Most components of the molecular machinery of actin-based motility have been identified [2, 3, 4]. It has been possible to perform experiments with reconstituted systems of Listeria propulsion [5, 6] for which detailed elastic models have been developed [7]. In vivo, cell spreading on matrix-coated surfaces provides a simplified system of analyzing motile behavior. A substantial amount of experimental and theoretical work has been done along these lines [8, 9, 10, 11]. However, only quite recently, quantitative experiments of whole cell spreading and subsequent migration could be performed with high spatial and temporal resolution [12, 13]. We found that there are well defined and distinct states of spreading. It is the goal of this work to show that these states can indeed be considered phases of motility by demonstrating the existence of dynamic phase transitions between them.

Spreading cells extend a 200 nm thick sheet called the lamellipodium from the cell body onto the substrate, see Fig. 1. This process is driven by actin polymerization at the leading membrane edge, the precise mechanism of which is still under debate [14, 15]. The meshwork of actin fibers is crosslinked by various proteins. The molecular motor myosin II enables the meshwork to contract by moving along actin fibers and relative to other cytoskeletal elements. Thus, the lamellipodium is an active gel enclosed in a flat membrane bag adhering to the substrate. The physics of active gels has recently attracted a lot of attention. Rheological experiments of simple mixtures of purified actin and myosin solutions [16] and quite general theoretical modeling [17, 18] have

been carried out. There are dynamic phase transitions involving extended and contracted actin density states as a function of myosin-actin coupling strength [17]. We will show that our cellular system exhibits similar transitions which express themselves prominently in the dynamics of the leading membrane edge.

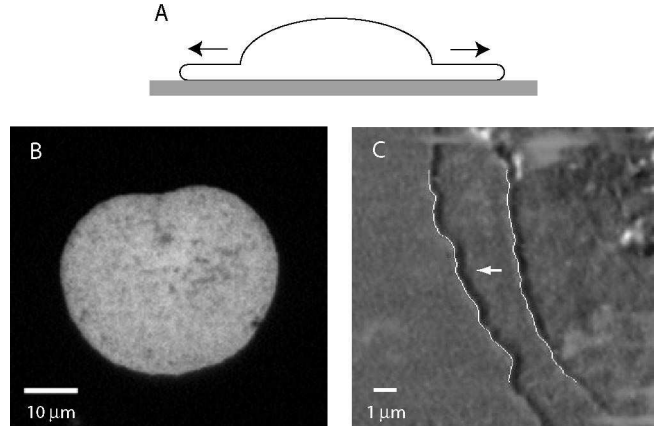


FIG. 1: A: During cell spreading, a thin lamellipodial sheet extends from the cell body onto the substrate. B: Total internal reflection fluorescence micrograph of a spreading cell. The bright region corresponds to the area adhered to the substrate. C: Two overlayed snapshots of the leading membrane edge of a lamellipodium moving from right to left are shown in differential interference contrast. The edge position is marked with a white contour overlay.

Mouse embryonic fibroblasts (MEF) were allowed to settle onto fibronectin coated glass slides and observed with either total internal reflection fluorescence (TIRF) or differential interference contrast (DIC) microscopy. Fibronectin links the cell membrane to the extracellular matrix proteins mimicking natural cell adhesion. TIRF studies were performed at a moderate spatial and tempo-

ral resolution to capture overall spreading characteristics of the whole cell. Multiple cells could be studied simultaneously. High resolution DIC was used to characterize local membrane dynamics. Details of the methods may be found in our earlier work [12, 13].

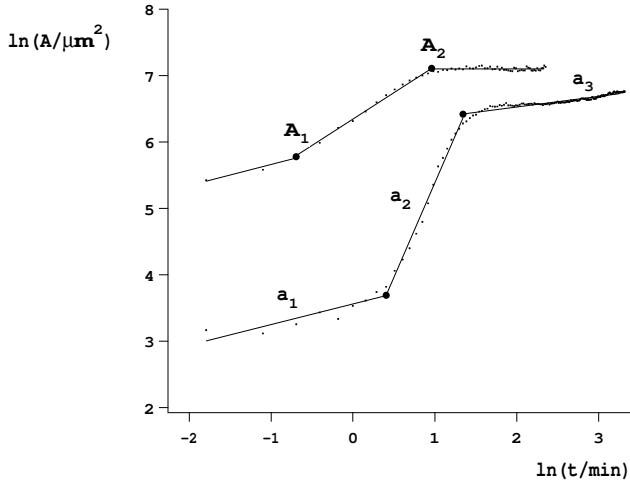


FIG. 2: Adhesion area in isotropically spreading fibroblasts grows with a power law in time. Different but constant exponents a_i in the various phases of spreading are evident in a double logarithmic plot. Exponents have been determined by fitting a piecewise linear function to the data, see Fig. 3. Adhesion areas A_i at the transition points are indicated.

Membrane adhesion area A during spreading was best monitored using TIRF. Distinct classes of angular isotropic and anisotropic spreading cells were found [12]. In the following, we limit ourselves to the isotropic class lacking filopodia. Close inspection of double logarithmic plots of adhesion area A over time reveals three phases with distinctly different power law growth, as seen in Fig. 2. We define area growth exponents a_i via

$$A(t) \sim t^{a_i}, \quad (1)$$

where i denotes the subsequent phases. Initially, there is a basal phase where cells test the suitability of the substrate to adhere and area growth is minimal. We find $a_1 = 0.4 \pm 0.2$. Then follows a phase of fast continuous spreading, which is characterized by $a_2 = 1.6 \pm 0.9$. Finally, the cell slows down again exhibiting a sub-linear area growth with $a_3 = 0.3 \pm 0.2$. We will see below that the latter phase is characterized by periodic local contractions of the cell [13]. Nevertheless, the mean area growth leads to an effective power law behavior also in this phase. Histograms of exponents a_i for the three phases are shown in Fig. 3. There is a clear distinction of fast area growth in the continuous spreading phase with a rather broad distribution of the exponent a_2 . However, we find two narrow clusters when discriminating with respect to the relative area growth, A_2/A_1 , during

that phase, where A_i denotes the adhesion area at the transition from phase i to $i + 1$. Small ($A_2/A_1 < 5$) or large ($A_2/A_1 > 5$) area increases correspond to small ($m_2 = 0.9 \pm 0.2$) or large ($m_2 = 1.6 \pm 0.2$) exponents, respectively. In addition, there were two single cells with even larger exponents m_2 which we excluded from the cluster average.

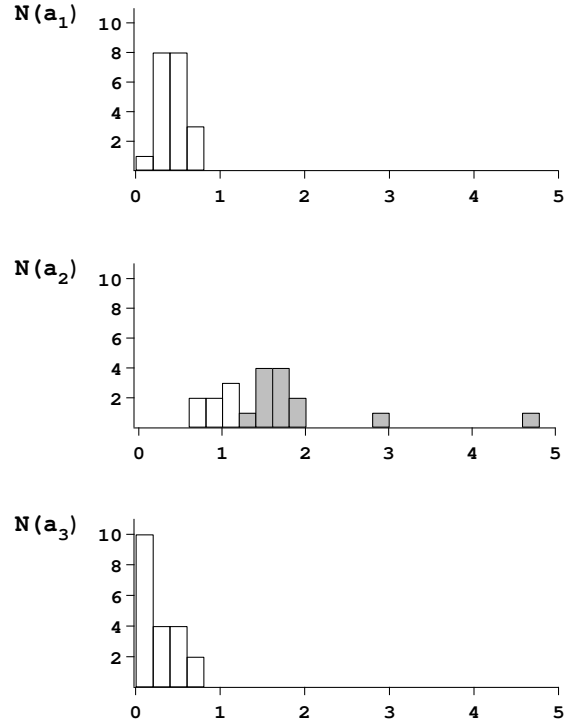


FIG. 3: Histograms of area growth exponents as obtained from the slopes of double logarithmic plots of adhesion area versus time, like the ones shown in Fig. 2. We have analyzed 20 cells in total. The middle (continuous spreading) phase exhibits clustering corresponding to small (open bars) and large (filled bars) area growth during that phase.

The transition from continuous to contractile spreading was further monitored using high resolution DIC. A suitable isotropically spreading cell was chosen and a well-resolvable and approximately straight membrane segment was selected for prolonged observation, see Fig. 1 B. Time-lapse sequences were obtained at video rate. Movies were digitized at $1/\Delta t = 3\text{Hz}$. Individual frames are counted using an index n . The cell edge is determined with a custom C program by a local contour algorithm [19] allowing nanometer accuracy. We obtain a sub-pixel resolution of 15 nm for relative displacements, which translates into a minimal detectable velocity of 45 nm/s between frames. Further analysis proceeds using a cartesian coordinate system where the average membrane orientation is taken as the fixed y -axis. Points on the membrane are then labeled by their y -coordinates y_j

and the membrane velocity $v_j(n) = \Delta x_j(n)/\Delta t$ is measured along the x-axis which is normal to the average membrane orientation.

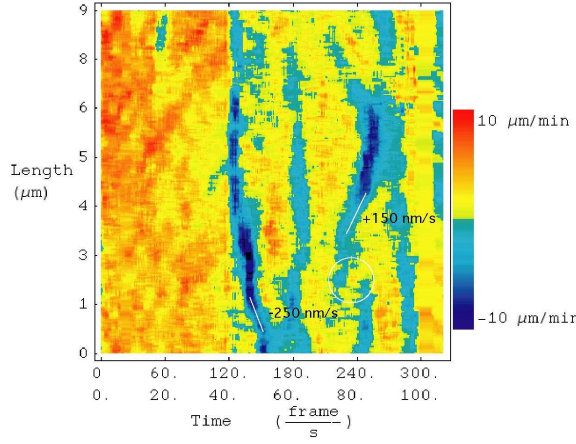


FIG. 4: Normal velocity map of the particular membrane segment marked in Fig. 1B as a function of time. Note the two qualitatively different sections before and after time $t = 40$ s corresponding to a continuous and a periodically contractile spreading phase, respectively. The period of the latter is $T = 17 \pm 4$ s. The speeds of lateral waves of maximum contraction velocity are indicated. The encircled region marks a phase shift of a contraction.

A typical velocity map along the contour over time is shown in Fig. 4. We find that a region of continuous, uninterrupted spreading (red shadows) precedes a sequence of periodic membrane retraction events (blue stripes). These two different states of membrane dynamics correspond to the continuous spreading and contractile phase of the lamellipodium, found above. The two phases can be clearly distinguished using the discrete Fourier transformation $v(s)$ of the velocity map $v(n)$ defined as

$$v_j(s) = \frac{1}{N} \sum_{n=1}^N v_j(n) \exp\left(2\pi i \frac{(n-1)(s-1)}{N}\right), \quad (2)$$

where N is the number of frames. Averages are taken over spatial regions of interest. The continuous spreading phase is characterized by a strong boundary maximum of the spectrum $|v_j(s)|$ at $s = 1$, see Fig. 5 A. In contrast, in the contractile phase the spectrum develops a pronounced peak at $s = s_{\max}$, see Fig. 5 B, which signals oscillatory behavior with a period

$$T = \Delta t \frac{N}{s_{\max} - 1}. \quad (3)$$

Thus, the peak position of the power spectrum serves as an excellent phase indicator. We calculate the spectrum inside a small time window - with a width on the order of the repeat time - and sweep across the phase

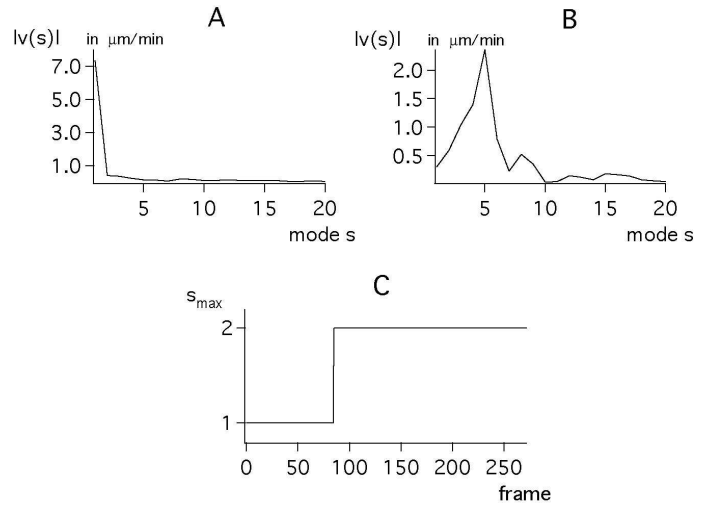


FIG. 5: Fourier spectrum (see Eq. 2) of the velocity map in Fig. 4 for the two different spreading phases below (A, $N = 120$) and above (B, $N = 200$) frame number $n = 120$. The spectrum is spatially averaged over 70 points between position $2.0 \mu m$ and $3.8 \mu m$ along the contour. The transition between continuous and contractile spreading is characterized by a sharp shift in the position of the maximum of the Fourier spectrum. The boundary maximum in panel A corresponds to a mean velocity of $7.4 \mu m$ in the continuous spreading phase. The peak at $s_{\max} = 5$ in panel B corresponds to a repeat time $T = 17 \pm 4$ s for the contractile spreading phase, see Eq. 3. The mean velocity $0.3 \mu m$ is small. The lower panel C depicts the peak position of the spectrum taken in a running time window with a width of $N = 50$ frames, corresponding to the repeat time T , as a function of the first frame number of the window. Note that the peak position depends on the width of the window used for Fourier transformation.

boundary. Indeed, there is a well defined transition between the two phases as seen in Fig. 5 C. However, the periodic contractions do not take place simultaneously along the leading edge, see Fig. 4. In fact, there are lateral waves of maximum contraction velocity running in both directions. These waves have a speed on the order of $200 nm/s$. Moreover, there are sudden phase shifts of the periodic contractions up to half a period, see encircled region in Fig. 4.

To summarize our experimental findings, we have seen clear signatures of dynamic phase transitions in the spreading behavior of MEF cells. Since actin polymerization does not stop during membrane retraction events [13], one concludes that the actin network contracts and/or is actively pulled back by myosin motor activity. Kruse et al. [17] have modeled oriented fibers connected into a network by molecular motors. They find an instability of homogeneous fiber density towards a contracted state as a function of fiber-motor coupling strength. Moreover, their generic theoretical model allows for oscillatory solutions. Our cellular system ex-

hibits similar behavior. Indeed, the periodic contractions are absent when myosin light chain kinase (MLCK), which activates myosin, is inhibited [13].

In the following, we give a systems biology oriented view of cell motility. Several questions arise: What is the functional role of the phases described above? How are these dynamic phases of the structural motility network regulated and connected to the signaling network? Can we disentangle the complex set of motility related proteins and simplify description by considering functional modules and hierarchical levels of control?

During the initial spreading phase, a MEF cell assembles the cytoskeletal structure necessary to probe the mechanical suitability of the substrate in the following contractile phase where it periodically pulls on the substrate. Indeed, cells require stiff substrates for growth and move toward stiffer regions [11]. The machinery for this stiffness sensing is organized into i) the basic structural elements consisting of the actin cytoskeleton, the myosin II motors, as well as the plasma membrane, ii) factors directly regulating protein coupling strength and activity, and, finally, iii) these regulatory proteins are controlled by a signaling network coordinating spatially distant and/or logically separate functional events in the cell. In order to link these cellular components to the physics of dynamic phase transitions, we note that it is the basic structural elements which exhibit the various phases we have identified in this work. The phase parameters are given by the regulating proteins, e.g., MLCK activity and concentration. The different dynamic phases correspond to functional regions in the regulating parameter space. The trajectories in this parameter space are determined by the cellular signaling network. This hierarchical identification provides an immediate conceptual advantage: The topology of the motility phase diagram is independent of the complex signaling network, i.e., the relative positions of all the motility phases do not depend on the trajectories in parameter space followed by the cell. Indeed, the basic phase characteristics can be probed and modeled separately. This was demonstrated using the observed linear relationship between the period of contractions and the lamellipodia width [13]. We find that the contraction period is the same for equal lamellipodia width, independent from the variations in the biochemical pathway(s) induced in order to achieve a certain width. On the other hand, cell motility is a unique case where the interconnections of the structural and signaling networks, which depend on gene expression, can be probed in order to establish a quantitative link between phenotype and genotype. We are currently identifying functional modules in a large scale screening of spreading phenotypes across various fibroblast cell lines with mutant genotypes.

The idea of phases in cell behavior can be applied quite generally. Phases of motility should be considered analogous to the phases of the cell cycle, phases of

varying metabolic activity or different protein expression. We propose to classify cellular behavior in well defined phases. Their number will be considerably less than an enumeration of concentration and activity levels of all molecular components of the cell. Thus, one can hope to accomplish a simplified description. Currently, phase classification is not generally done and cellular phenotype cannot be sensibly compared across different genotypes. We expect that some fraction of the variability encountered in biological experiments and the often conflicting results between laboratories stem from the fact that findings corresponding to different cellular phases and boundary conditions are spuriously compared to each other. In conclusion, we feel that the classification of motility in phases can serve as a paradigmatic example for a powerful general ordering principle in quantitative biology.

This work was funded by the Deutsche Forschungsgemeinschaft and the National Institutes of Health via grant GM 036277. HGD would like to thank Adam Meshel and Ana Kostic for helpful discussions.

* Electronic address: hgd@biology.columbia.edu

- [1] D. Bray, *Cell movements: From Molecules to Motility*, Garland Publishing, 2nd Ed. (2001).
- [2] T. P. Stossel, Science **260**, 1086 (1993).
- [3] D. Pantaloni, C. Le Clainche, M-F. Carlier, Science **292**, 1502 (2001).
- [4] T. D. Pollard, G. G. Borisy, Cell **112**, 453 (2003).
- [5] A. Bernheim-Grosswasser, S. Wiesner, R.M. Golsteyn, M-F. Carlier, C. Sykes, Nature **417**, 308 (2002).
- [6] A. Upadhyaya, A. van Oudenaarden, Current Biology **13**, R734 (2003).
- [7] F. Gerbal, P. Chaikin, Y. Rabin, J. Prost, Biophys. J. **79**, 2259 (2000).
- [8] M. Dembo, Y.-L. Wang, Biophys. J. **76**, 2307 (1999).
- [9] Balaban et al., Nature Cell Biology, **3**, 466 (2001).
- [10] G. Jiang, G. Giannone, D. R. Critchley, E. Fukumoto, M. P. Sheetz, Nature **424**, 334 (2003).
- [11] I. B. Bischofs, S. A. Safran, U. S. Schwarz, Phys. Rev. E **69**, 021911 (2004).
- [12] B. Dubin-Thaler, G. Giannone, H.-G. Döbereiner, and M. P. Sheetz, Biophys. J. **86**, 1794 (2004).
- [13] G. Giannone, B. Dubin-Thaler, H.-G. Döbereiner, and M. P. Sheetz, Cell **116**, 431 (2004).
- [14] R. B. Dickinson and D. L. Purich, Biophys. J. **82**, 605 (2002).
- [15] A. Mogilner and G. Oster, Biophys. J. **84**, 1591 (2003).
- [16] D. Humphrey, C.Duggan, D.Saha, D.Smith and J.Käs, Nature **416**, 413 - 416 (2002).
- [17] K. Kruse, F. Jülicher, Phys. Rev. E **67**, 051913 (2003).
- [18] K. Kruse, J. F. Joanny, F. Jülicher, J. Prost, K. Sekimoto, Phys. Rev. Lett. **92**, 078101 (2004).
- [19] H.-G. Döbereiner, E. Evans, M. Kraus, U. Seifert, M. Wortis, Phys. Rev. E **55**, 4458 (1997).